X-ray absorption measurement and density functional theory analysis of gallium in gallium-containing beta zeolites

ARTICLE *in* MICROPOROUS AND MESOPOROUS MATERIALS · OCTOBER 2001

Impact Factor: 3.45 · DOI: 10.1016/S1387-1811(01)00323-7

5 AUTHORS, INCLUDING:

Pang-Hung Liu
Industrial Technology Research Institute
20 PUBLICATIONS **456** CITATIONS

SEE PROFILE

ELSEVIER

Microporous and Mesoporous Materials 47 (2001) 147–156

MICROPOROUS AND MESOPOROUS MATERIALS

www.elsevier.com/locate/micromeso

X-ray absorption measurement and density functional theory analysis of gallium in gallium-containing beta zeolites

An-Chyi Wei [a], Pang-Hung Liu [a], Kuei-Jung Chao [a,*], Esther Yang [b], Hsiu-Yao Cheng [b]

[a] *Department of Chemistry, National Tsinghua University, Kuang Fu Road, Hsinchu 30043, Taiwan, ROC*
[b] *Department of Chemistry, Tunghai University, Taichung, Taiwan, ROC*

Received 16 January 2001; received in revised form 10 May 2001; accepted 10 May 2001

Abstract

The chemical states and coordination geometries of Ga species in Ga/H[Si,Al]-beta (prepared by impregnation) and [Si,Ga]-beta (prepared by hydrothermal synthesis) before and after in situ redox treatments were determined by Ga K-edge X-ray absorption spectroscopy, and confirmed by density functional theory calculation.

Keywords: Hydrothermal synthesis; Impregnation; Ga-beta; XAS; ^{71}Ga-NMR; Density functional theory

1. Introduction

Gallium-doped zeolites were found active in the transformation of light alkanes into aromatics and in the dehydrogenation or oxidative dehydrogenation of alkanes [1,2]. During aromatization, a synergism between the gallium metal and the acidity of zeolites was observed. The highly dispersed gallium in the pores of zeolites was assumed to play the key role in both reaction selectivity and activity [3,4]. Techniques such as hydrothermal synthesis, impregnation, ion exchange and mechanical mixing have been used to introduce gallium into zeolites. After the synthesis, part of the gallium was found to be incorporated into the zeolitic framework, and a thermal activation treatment extracted the metal from the framework to give non-framework gallium species. The nature and the variation of framework and non-framework gallium under various reaction conditions [4–6] are not only scientifically interesting but also important for both the understanding and the development of the aromatization of light paraffins. Spectroscopic characterizations, e.g., by XRD and ^{29}Si- and ^{71}Ga-NMR, were employed to probe the post-synthesis incorporation of Ga in the zeolite framework [1,5–8].

Since the amount of framework-incorporated gallium is usually low, X-ray absorption spectroscopy (XAS) could be a sensitive enough tool to investigate the local structure of gallium ions by providing both the bonding parameters of central ions to the adjacent atoms and the oxidation states of the central metal. In the present study, *in situ* XAS (XANES and EXAFS) was used to probe the nature of gallium species in hydrothermally

* Corresponding author. Fax: +886-3-5720964.
E-mail address: kjchao@mx.nthu.edu.tw (K.-J. Chao).

1387-1811/01/$ - see front matter
PII: S1387-1811(01)00323-7

synthesized ([Si,Ga]-beta), incipient-impregnated (Ga/H[Si,Al]-beta) and these samples after redox treatments. The presence of gallium in the framework of zeolite beta is also verified by cluster modeling and quantum chemical calculation based on density functional theory (DFT). During the calculation, full and constrained geometry optimizations have been performed and the calculated results are compared with EXAFS data.

2. Experimental

2.1. Sample preparation and characterization

[Si,Ga]-beta zeolite was synthesized under hydrothermal conditions from a gel with the molar compositions 0.2:1:0.0025–0.008:0.1:15 = $(TEA)_2O$:SiO_2:Ga_2O_3:Na_2O_3:H_2O. The reactants were fused silica (Aldrich, Aresol 200), sodium hydroxide (Riedeal-de Häen), tetraethylammonium hydroxide, TEAOH (35% aqueous, Aldrich) and gallium nitrate (Kojundo, 99.9%) with deionized water. The pH of the reactant gel was between 12.9 and 13.8. The homogeneous gels were heated in Teflon-lined autoclaves for 8–14 days at 135°C. The as-synthesized sample (TEA form) was washed and dried at 80°C and then changed to the H,Na form by heating at 550°C for 10 h in steam-loaded air. NH_4 [Si,Ga]-beta was obtained from the H,Na form by a six-fold ion exchange with 1 N NH_4Cl solution at 70°C. Finally, NH_4 [Si,Ga]-beta was calcined to form H[Si,Ga]-beta. Ga/H[Si,Al]-beta was prepared by the incipient wetness impregnation method. An aqueous $Ga(NO_3)_3 \cdot 9H_2O$ (Kojundo) solution was added dropwise to H-BEA zeolite (P.Q. Corp., Si/Al = 14), the resulting solid was dried overnight in air at room temperature, and then at 80°C for 2–3 h, and further calcined at 500°C for 3 h under a flow of air. The Si/Al ratio in both [Si,Ga]-beta and Ga/H[Si,Al]-beta was 14 corresponding to a gallium content of ~1 wt.%, as determined by inductively coupled plasma-atomic emission spectroscopy (ICP-AES). Samples were examined by XRD on a powder diffractometer (Rigaku DMX II) with Cu Kα radiation. ^{71}Ga MAS NMR spectra were recorded on a Bruker DSX-400 instrument. $Ga(NO_3)_3$ solution was employed as an external standard. Typically, 16,000 free induction decays were accumulated with a flip angle produced by 3 μs excitation pulses and intervals of 1 or 0.5 s. The rotor was spun at 12 kHz. Beta zeolite was the only crystalline product observed in the XRD patterns of both [Si,Ga]-beta and Ga/H[Si,Al]-β. Since only tetrahedral Ga at ~156 ppm appears in the ^{71}Ga NMR spectra (Fig. 1) of as-synthesized [Si,Ga]-beta and calcined Ga/H[Si,Al]-beta, their Ga species can thus be considered to reside in framework positions.

2.2. X-ray absorption spectroscopy

XAS measurements were performed on the beamline BL17C at the Synchrotron Radiation Research Center (SRRC), Taiwan, with a storage ring energy of 1.5 GeV and a beam current between 120 and 200 mA.

Prior to the XAS measurements, the calcined, hydrated sample was mounted in an *in situ* cell [9], and then heated from room temperature to 350°C at 5°C/min, and this temperature was maintained for 2 h under a He flow to remove adsorbed water. The dehydrated and calcined sample was then cooled down to room temperature under a He flow before the XAS measurement. The calcined, dehydrated sample was heated again from room temperature to 550°C at 5°C /min under He flow, He was then replaced by H_2 to effect reduction at 550°C for 2 h. The reduced sample was cooled down to room temperature either under a hydrogen or a helium flow.

The X-ray absorption spectra were measured in the transmission mode at the Ga K-edge at room temperature. The energy was scanned from 200 eV below the gallium K absorption edge (10 375 eV) to 1100 eV above the edge. Standard Ga_2O_3 powder was used as a reference and measured simultaneously with the samples so that an energy calibration could be done between the scans.

The EXAFS data were analyzed by curve fitting using the UWXAFS 3.0 software package [10] and the FEFF6 [11] program. The EXAFS oscillation $\chi(E)$ in energy space was extracted from the experimentally measured absorption coefficient $\mu(E)$

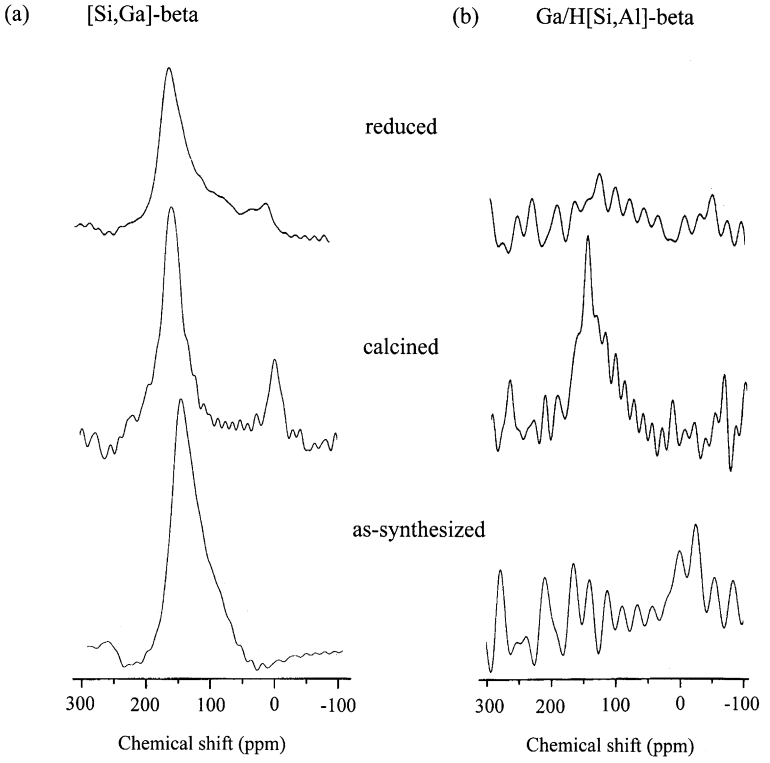

Fig. 1. ^{71}Ga MAS NMR spectra of [Si,Ga]-beta samples (a) and Ga/H[Si,Al]-beta samples (b).

by subtracting an isolated atom-like background absorption function $\mu_0(E)$, using the relation $\chi(E) = (\mu(E) - \mu_0(E))/\mu_0(E)$. Subsequently, $\chi(E)$ was converted into a k-space function $\chi(k)$, where k is the wave number of an ejected photo-electron given by $k = 2\pi(2m_e(E - E_0)/h^2)^{1/2}$, where m_e is the mass of electron. A typical EXAFS function $\chi(k)$ contains some structural parameters such as: N_j, the coordination number of the jth shell, R_j, the interatomic distance, σ_j^2, the Debye–Waller factor. These useful structural parameters can be obtained by curve-fitting. Both k^2- and k^3-weighted Fourier transformations, without phase shift corrections, were performed. The k^3-weighted Fourier transforms in r (distance) space on the EXAFS data are described.

Curve-fitting procedures began with the ab initio calculation of the phase shift and amplitude functions for single-scattering of atom pairs using the FEFF6 program. As for the input to FEFF6, we used a known atom cluster from the reference compound Ga_2O_3 and interatomic distances from the published crystal structure. Theoretical phase shift and amplitude functions were obtained for atom pairs including: Ga–O (GaO_4 in Ga_2O_3), Ga–O (GaO_6 in Ga_2O_3), Ga–Ga (Ga–O–Ga in Ga_2O_3), Ga–Ga in Ga metal. As for the unknown species of Ga$\cdots$Si pair (proposed in this paper), its theoretical function was obtained by using FEFF6 for Me–L of MeL_6 octahedra (where Me is the central absorber atom and L is the coordinating atom). The fitting between the theoretical and experimental data was made in r-space within the range of a specific profile. The good-fit parameter, denoted as R-factor, was always found to be below 0.02.

3. Computational method

Calculations based on DFT [12] were carried out using the B3LYP hybrid method involving a

three-parameter Becke exchange functional [13] and a Lee–Yang–Parr correlation functional [14]. All calculations were performed using a GAUSSIAN98 program [15].

Various cluster models were considered, and each represented a framework (T = Al, Si or Ga) site of zeolite beta in which the Ga resided. The models were divided into two categories according to their geometry optimization. The first category consisted of three dimer models representing the calcined and reduced forms in [Si,Ga]-beta and Ga/H[Si,Al]-beta. Model Ia stands for a Ga^{3+} ion in the tetrahedral framework and consists of $(HO)_3GaOHSi(OH)_3$. Model Ib1 stands for a Ga^{3+} ion connected to a silanol group on the beta surface and consists of $(H_2O)(HO)_2GaOSi(OH)_3$. Model Ib2 stands for the $Ga(H_2O)_3^{1+}$ species being reduced from model Ib1 and consists of $(H_2O)_3$-$GaOSi(OH)_3$. The full geometry optimization (FOPT) using the 6-311++G** basis set was performed for this category.

The framework structure of zeolite beta is known to contain three mutually intersecting 12-ring channel systems and to be built from layer-like tetragonal building units, the periodic building unit being composed of 16 tetrahedra (T) related by pure translations along the *a* and *b* axes [16–18]. The smaller building units are double six-ring units connected by two four-rings and four five-rings. These are connected to form chains along the [0 0 1] direction. Polymorphs A and B contain nine topologically different T sites, T_1–T_9, shown in the $1 \times 1 \times 1$ cell cluster of the BEA framework of Fig. 2b, whereas polymorph C contains 32 unique

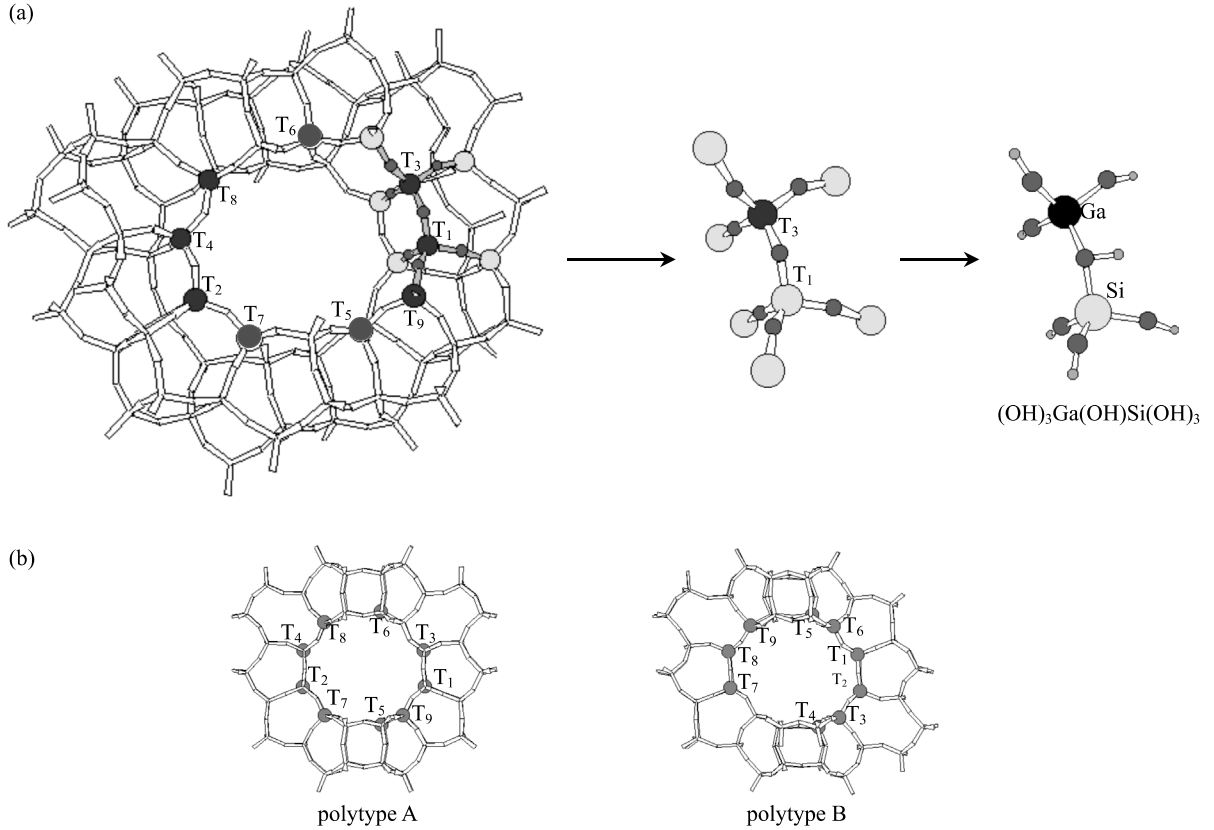

Fig. 2. (a) Schematic representation of the generation of dimer models of the second category from polytype A of the beta framework. (b) 12-rings viewed along [1 0 0] of polytype A (loop configuration of T-atoms: ⊔ for T_{1-4}, ⊓ for T_{5-6} and ⊥ for T_{7-9}) and [1 1 0] of polytype B (loop configuration of T-atoms: ⊔ for T_{1-2} and T_{7-8}, ⊓ for T_{4-5} and ⊥ for T_3, T_6 and T_9).

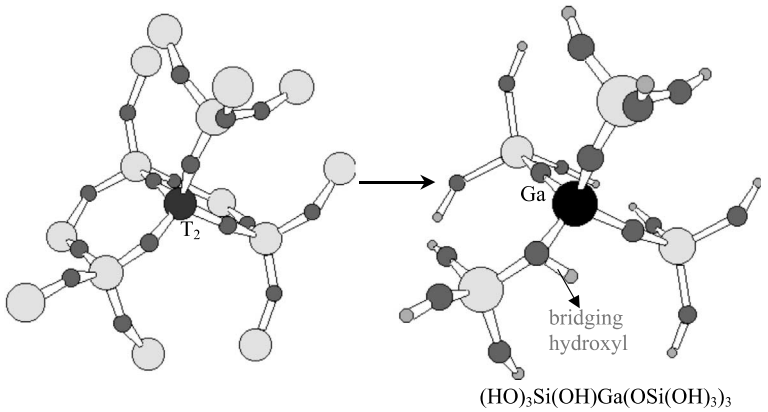

Fig. 3. Schematic representation of the generation of pentamer models of the second category.

T sites [16]. In order to find a favorable location for Ga^{3+} to reside, the partial geometry optimizations (POPT) are employed for the second category of models due to the restrictions of the framework structure. These models represent the calcined forms of [Si,Ga]-beta with both dimer and pentamer taken into consideration. To generate the dimer model, the CERIUS^2 program package [19] was invoked to load the $1 \times 1 \times 1$ unit cell structure of polymorph A of zeolite beta [20]. First, the cluster of the expanded $2 \times 2 \times 2$ cell was built. Then, one silicon atom in a T site was substituted by one gallium atom, and the corresponding $O_3GaOSiO_3^{7+}$ dimer cluster was removed. In the next step, all the dangling bonds due to such a cutting were saturated with hydrogen atoms along the framework directions, and the OH bond distances were adjusted to 0.96 Å to avoid the boundary effect. The counter-ion, H^+, was added to the bridge O, and each dimer model of the second category consisted of $(HO)_3Ga(OH)Si(OH)_3$. The procedures of building the pentamer clusters were similar to those of the dimer clusters. To sum up, the $Ga(OSiO_3)_4^{13-}$ pentamer cluster was removed after one Si atom in a T site was substituted by the Ga atom, and all the dangling bonds were saturated with hydrogen atoms with adjusted bond lengths of 0.96 Å along the framework directions. Each T site is surrounded by four non-equivalent oxygen atoms. Thereby, four possible bridging hydroxyl configurations with regard to each T site can be generated. Based on our previous work [5], the possible bridging hydroxyl H atom is connected to the O atom with the smallest T–O–T angle. Notice that the Ga atom was in the center of the $(HO)_3Si(OH)Ga(OSi(OH)_3)_3$ cluster.

In the dimer and pentamer models, the Ga^{3+} or Al^{3+} ion was chosen to reside in one of the T_1–T_9 sites (Figs. 2 and 3). Note that POPT was carried out on models of the second category under the symmetry restriction that the positions of terminal hydroxyl groups were fixed and the OH bond distances were set to 0.96 Å. The 6-311++G** and 6-31G basis set were empolyed for the dimer and pentamer calculations, respectively.

4. Result and discussion

4.1. Ga K-edge XANES

Normalized Ga K-edge XANES spectra of as-synthesized, calcined and dehydrated and reduced and dehydrated [Si,Ga]-beta samples are compared with that of Ga_2O_3, in Fig. 4. The XANES spectrum of Ga_2O_3 powder consists of a broad peak at the edge (10 375.0 eV) that is associated with four coordinated Ga^{3+} and a peak at an energy approximately 3 eV higher and is associated with the six coordinated Ga^{3+}, consistent with those obtained by Nishi et al. [21]. The edge energies of as-synthesized and calcined, dehydrated [Si,Ga]-beta samples of 10 374.5–10 375.0 eV are

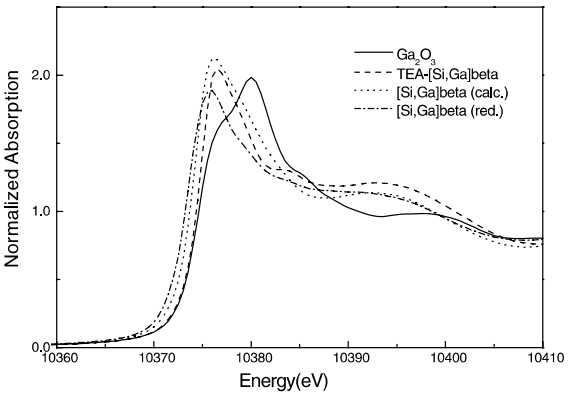

Fig. 4. Ga K-edge XANES spectra of [Si,Ga]-beta samples.

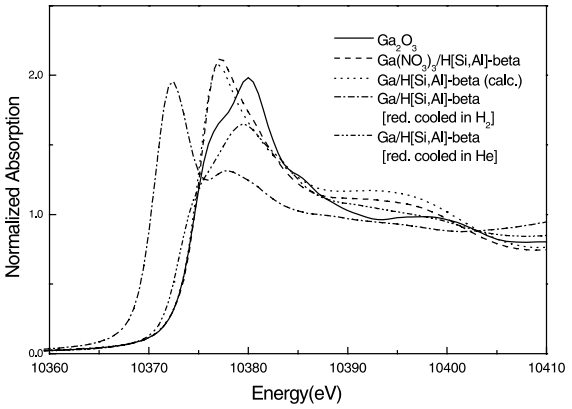

Fig. 5. Ga K-edge XANES spectra of Ga/H[Si,Al]-beta samples.

close to that of four-coordinated Ga^{3+} in Ga_2O_3 (10 375 eV) as shown in Table 1 and Fig. 4. This suggests that the gallium ions in as-synthesized and calcined [Si,Ga]-beta samples are predominantly in the 3+ state and a coordination number of four. The edge energy of reduced and dehydrated [Si,Ga]-beta (cooled in H_2) was found to be 10 373.5 eV, indicating that some Ga^{3+} species were reduced.

Fig. 5 shows that the as-prepared and the calcined, dehydrated Ga/H[Si,Al]-beta samples have their edge energies similar to that of tetrahedral Ga^{3+} in Ga_2O_3 (10 375.0 eV). The edge energy of the XANES profile of the reduced, dehydrated Ga/H[Si,Al]-beta sample (cooled in H_2) is 10 370.5 eV lower than that of the reduced, dehydrated Ga/H[Si,Al]-beta sample (cooled in He) (10 373.0 eV). The profile of the reduced, dehydrated Ga/H[Si,Al]-beta sample (cooled in H_2) consists of one strong peak and one weak peak in the near-edge region, a possible indication of partial reduction of Ga from 3+ to 1+. This was also detected by TPR measurements [22]. The present *in situ* XANES investigations indicate that the state of Ga is dependent on the reduction and the cooling conditions.

4.2. Ga K-edge EXAFS

Fourier transforms of $k^3\ \chi(k)$ Ga K-edge EXAFS spectra of [Si,Ga]-beta and Ga/H[Si,Al]-beta samples and results from curve-fitting are compared with that of Ga_2O_3 and $Ga(NO_3)_3$/H[Si,Al]-

Table 1
Ga K-edge EXAFS results of [Si,Ga]-beta and Ga/H[Si,Al]-beta samples

Sample	Edge (eV)	Shell	Distance (Å)	CN	σ^2 (Å^2) $\times 10^{-3}$
TEA-[Si,Ga]-beta	10 375.0	Ga–O	1.81	3.9	2
[Si,Ga]-beta (calc.)	10 374.5	Ga–O	1.82	4.1	6
		Ga–Si	3.06	0.7	0.5
		Ga–Si	3.47	1.0	7
[Si,Ga]-beta (red.)	10 373.5	Ga–O	1.79	3.8	7
		Ga–Si	3.11	0.9	0.1
		Ga–Si	3.41	0.2	7
$Ga(NO_3)_3$/H[Si,Al]-beta	10 375.0	Ga–O	1.84	5.4	8
Ga/H[Si,Al]-beta (calc.)	10 375.0	Ga–O	1.82	3.9	4
Ga/H[Si,Al]-beta (red. cooled in H_2)	10 370.5	Ga–O	1.92	1.4	14
		Ga–Si	3.15	1.1	11
Ga/H[Si,Al]-beta (red. cooled in He)	10 373.0	Ga–O	1.88	3.8	17

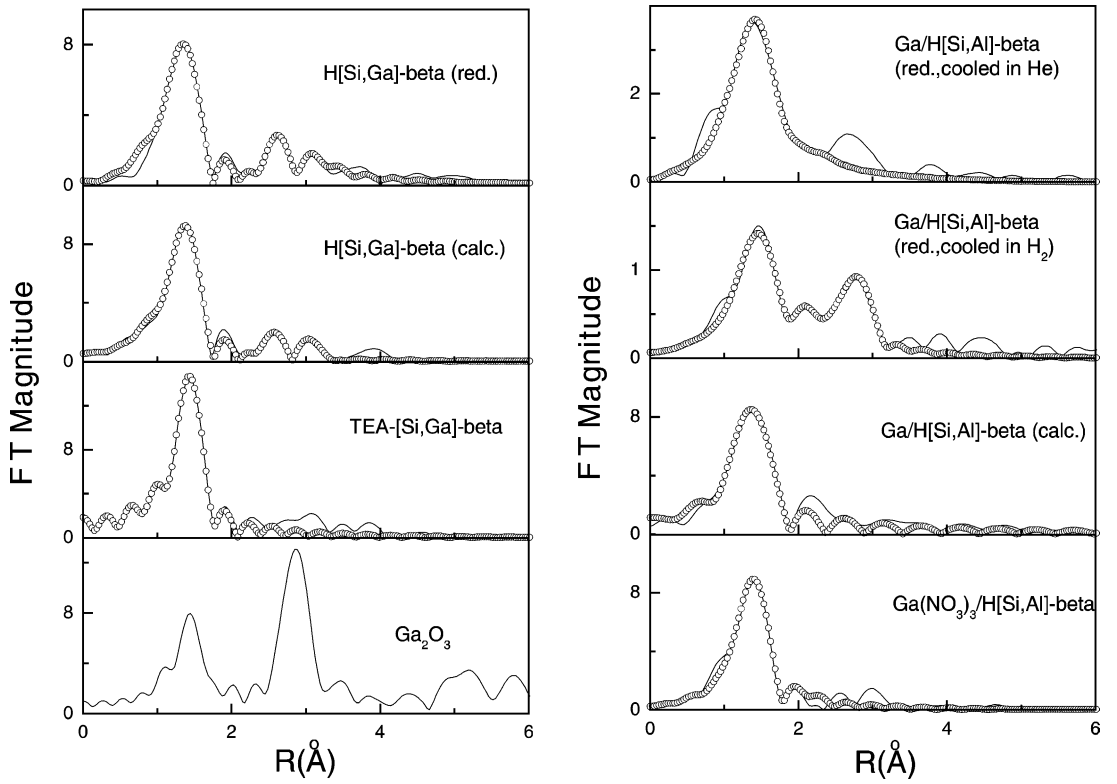

Fig. 6. Fourier transforms of Ga K-edge k^3-weighted EXAFS data for [Si,Ga]-beta and Ga/H[Si,Al]-beta samples. Solid lines and open circles are the experimental and the fitted results, respectively. Note that the phase shifts were not corrected.

beta in Fig. 6, and the structural parameters thus derived are given in Table 1. Ga_2O_3 consists of tetrahedral Ga–O with a bond distance of 1.86 Å and octahedral Ga–O with a bond distance of 1.98 Å with Ga–O–Ga species of shortest Ga–Ga distances at 3.07 or 3.37 Å as described in our previous work [23] and consistent with single crystal XRD results [24]. In Fig. 6 and Table 1 the intense peak of [Si,Ga]-beta, at about 1.8 Å corresponds to GaO_4 of four oxygen atoms (CN = 3.9, 4.1 or 3.8) around a Ga atom at a distance of Ga–O = 1.79–1.82 Å, while the two weak peaks at 3.1 and 3.4–3.5 Å are assigned to Ga–O–Si. No identifiable Ga–Ga peak of Ga–O–Ga was observed. These findings show that tetrahedral Ga atoms are separately incorporated into the zeolitic framework. These isolatedly dispersed framework Ga^{3+} ions are stable even under redox treatment at high temperature. This is consistent with the XANES results shown before. The corresponding ^{71}Ga MAS NMR profiles of all [Si,Ga]-beta samples in Fig. 1(a) show tetrahedral Ga peaks at ~151 ppm, confirming that Ga of [Si,Ga]-beta zeolites may reside in the framework position.

Table 1 shows a coordination number (CN) of 5.4 and bond distances (d(Ga–O)) of 1.8 Å for the first shell atoms around Ga^{3+} ions of as-prepared Ga/H[Si,Al]-beta, close to that of octahedral Ga^{3+} ions in $Ga(NO_3)_3$ [25] doped on beta. They were found to be converted to tetrahedral Ga^{+3} species of d(Ga–O) = 1.82 Å and CN = 3.9 after calcination treatment. However, such $Ga^{3+}O_4$ species of Ga/H[Si,Al]-beta was not as stable as that in [Si,Ga]-beta during the high-temperature reduction and cooling process. The presence of the Ga–O distance of 1.92 Å and CN = 1.4 together with a Ga–O–Si at d(Ga–Si) = 3.15 Å and CN (Ga–Si) = 1.1 on reduced sample suggests that

Ga ions could either fall out of tetrahedral sites or change to other forms. EXAFS of reduced Ga/H[Si,Al]-beta (cooled in H_2) shows Ga–O and Ga–Si peaks at <3.2 Å instead of one major Ga–O peak at about 1.88 Å (CN = 3.8) for the reduced Ga/H[Si,Al]-beta zeolite (cooled in He). The ^{71}Ga MAS NMR spectra (Fig. 1(b)) showed a tetrahedral Ga peak at 151.4 ppm only for the calcined Ga/H[Si,Al]-beta zeolite but not for reduced and as-prepared Ga/H[Si,Al]-beta samples. The features of ^{71}Ga MAS NMR suggest that the reduced Ga species may have lost their symmetric coordination during reduction, and Ga^{3+} ions might be incorporated into different tetrahedral sites when different preparation methods are used. Ga ions might be introduced into defect sites of the framework (such as the silanol groups) through calcining the impregnated sample. Furthermore, they may not be stable under high-temperature reduction treatments.

4.3. Model calculation

In order to confirm the structures of Ga species and the location of Ga in the framework of zeolite beta, the calculated bond parameters for optimized cluster models are compared with the XAS results.

Table 2 gives the calculated Ga–O and Ga–Si bond distances and total energies of the models in the first category when the 6-311++G** basis set is used. As for the bond distances, the optimized Ga–O distances of both models Ia and Ib1 are in good agreement with the experimental EXAFS results. This suggests that Ga^{3+} ions can either be incorporated into tetrahedral sites or interact with silanol groups. However, none of the Ga–O–Si contributions to the bond distances at 3.06, 3.11, 3.41 and 3.47 Å from the EXAFS results could be reconciled with a simplified dimer model. The contribution of Ga–O–Si from a Ga atom connected to four nearby silicate sites in the zeolite framework cannot be explained by simple dimer models. The shortest Ga–Si distance is 3.5 Å in [Ga,Si]MFI zeolites as suggested by Okabe and Matsuboayashi [26].

Table 2
Bond distances (Å) of Ga–O and Ga–Si bonds and total energies (Hartrees) for the first category of dimer models in [Si,Ga]-beta and Ga/H[Si,Al]-beta[a]

Model	R_{Ga-O} (Å)	R_{Ga-Si} (Å)	Energy
Ia	1.80, 1.83, 1.84, 2.04	3.21	−2745.68
Ib1	1.79, 1.82, 1.82, 2.08	3.00	−2745.75
Ib2	1.86, 1.87, 2.28, 2.29	3.07	−2746.87

[a] Results obtained from the FOPT method.

For model Ib2, the optimized structure is similar to a $(H_2O)_2(H)(OH)GaOSi(OH)_3$ cluster with two short Ga–O bonds (1.87 and 1.86 Å) and two longer Ga–O bonds (2.28 and 2.29 Å) with a Ga–Si distance of 3.07 Å. The EXAFS feature of reduced Ga/H[Si,Al]-beta (cooled in H_2) corresponds to a structure with Ga–O bonds of 1.92 Å and a Ga–Si contribution of 3.15 Å.

The decrease in the coordination number of Ga–O bonds in reduced Ga/H[Si,Al]-beta (from 3.8 to 1.4) may be accounted for partially by bonding of gallium to framework oxygens. In view of the optimized Ga–O distances of 2.28 and 2.29 Å of the reduced dimer cluster, we are inclined to propose that Ga^+ ions can be solvated by the wall of the beta channels. It is noteworthy that the amplitude of the first EXAFS peak of the dehydrated, reduced Ga/H[Si,Al]-beta samples (cooled in H_2 or He) is considerably lower than that in the dehydrated, calcined Ga/H[Si,Al]-beta zeolite. Such a low amplitude may correspond to a fraction of gallium being reduced to its elementary form, the presence of Ga metal on Pt particles and gallium hydride species was observed on reduced Pt/Ga/H[Si,Al]-beta [23].

In the dimer models of the second category, after going through POPT calculations, the calculated Ga–O distances and Ga–Si distances are not in agreement with those of the EXAFS results. All these optimized models give one long Ga–O bond of 3.1 Å and a Ga–Si bond of 4.3 Å.

The calculated distances of Ga–O, Ga–Si, Al–O and Al–Si and the energies of the optimized pentamer models of [Si,Ga]-beta and [Si,Al]-beta using the POPT method are listed in Table 3. The relative energies, ΔE_r (refer to the cluster T9) of these sites are spread in the range of 222 kJ/mol. For [Si,Al] and [Si,Ga]-beta samples, the most stable T sites are T_7, T_8 and T_9. These three T sites are not involved in any four-rings, whereas T_{1-4} are connected two a four-rings loop and T_{5-6} have

Table 3
Bond distance (Å) of Ga–O, Ga–Si, Al–O and Al–Si and total energies (Hartrees) for the pentamer models of [Si,Ga]-beta and [Si,Al]-beta

[Si,Ga]-beta	d_{Ga-O} (Å)	d_{Ga-Si} (Å)	E_T[a]	ΔE_r[b]
T_1	1.73, 1.74, 1.75, 1.87	3.01, 3.14, 3.15, 3.32	−4292.28	221.84
T_2	1.73, 1.73, 1.75, 1.86	3.02, 3.14, 3.14, 3.32	−4292.29	204.51
T_3	1.74, 1.75, 1.75, 1.88	2.96, 3.13, 3.16, 3.36	−4292.29	209.24
T_4	1.74, 1.74, 1.75, 1.87	2.96, 3.13, 3.16, 3.30	−4292.29	208.20
T_5	1.74, 1.74, 1.75, 1.86	3.05, 3.08, 3.24, 3.28	−4292.32	115.77
T_6	1.74, 1.74, 1.75, 1.86	3.05, 3.07, 3.24, 3.29	−4292.32	122.59
T_7	1.74, 1.74, 1.75, 1.87	3.05,3.14, 3.17, 3.22	−4292.39	27.82
T_8	1.75, 1.75, 1.75, 1.87	3.00, 3.15, 3.18, 3.18	−4292.37	2.89
T_9	1.74, 1.74, 1.75, 1.86	3.04, 3.18, 3.20, 3.20	−4292.37	0
[Si,Al]-beta	d_{Al-O}	d_{Al-Si}	E_T[a]	ΔE_r[b]
T_1	1.68, 1.68, 1.69, 1.82	3.02, 3.12, 3.16, 3.28	−2611.90	194.01
T_2	1.68, 1.68, 1.69, 1.82	3.03, 3.12, 3.16, 3.28	−2611.91	169.08
T_3	1.68, 1.68, 1.69, 1.82	3.03, 3.12, 3.16, 3.28	−2611.92	157.78
T_4	1.68, 1.69, 1.70, 1.83	2.96, 3.14, 3.15, 3.26	−2611.91	182.21
T_5	1.68, 1.68, 1.69, 1.81	3.07, 3.11, 3.20, 3.26	−2611.95	79.83
T_6	1.68, 1.68, 1.69, 1.81	3.07, 3.10, 3.20, 3.27	−2611.95	87.95
T_7	1.69, 1.69, 1.69, 1.82	3.05, 3.14, 3.15, 3.21	−2611.98	2.09
T_8	1.69, 1.69, 1.70, 1.83	3.01, 3.15, 3.16, 3.18	−2611.98	6.57
T_9	1.69, 1.69, 1.69, 1.82	3.04, 3.18, 3.18, 3.20	−2611.98	0

[a] Total energies (Hartrees).
[b] Relative energies (kJ/mol) referred to the cluster T_9.

one four-ring loop. In polymorph B, T_3, T_6 and T_9 are not connected to a four-ring loop (Fig. 2b) and are expected to be the proper sites for hetero-atom incorporation. The calculated Ga–O and Ga–Si distances of those sites are in very good agreement with the EXAFS results.

Table 4 shows that the simulated bridging hydroxyl vibration frequencies are close to those in our previous experimental IR. spectra [5], i.e. the Ga(OH)Si group of [Si,Ga]-beta at 3619 cm^{-1} and the Al(OH)Si group of [Si,Al]-beta at 3607 cm^{-1}, respectively. Only for the T_7, T_8 and T_9 sites, the calculated value of the OH band for Ga(OH)Si in [Si,Ga]-beta is higher than that of Al(OH)Si in [Si,Al]-beta. This also suggests that Ga may be located on T_7, T_8 and T_9 sites.

Table 4
Simulated vibration frequency (cm^{-1}) of the bridging hydroxyl of the pentamer clusters

T site	ν_{O-H}	
	$(HO)_3Si(OH)Al(OSi(OH)_3)_3$	$(HO)_3Si(OH)Ga(OSi(OH)_3)_3$
T_1	3732.3	3730.4
T_2	3734.7	3730.9
T_3	3732.9	3730.9
T_4	3733.4	3730.9
T_5	3717.6	3690.8
T_6	3720.0	3698.9
T_7	3738.2	3741.6
T_8	3734.5	3738.6
T_9	3723.9	3729.9
Expt'l O–H frequency	3607	3619

5. Conclusion

This study demonstrated that the combination of *in situ* XAS measurements and DFT calculations is effective in determining the structure of heteroatoms in zeolites. The structure thus derived indicates that Ga atoms can be incorporated into different tetrahedral sites using different synthesis methods.

References

[1] J.M. Thomas, X.S. Liu, J. Phys. Chem. 90 (1986) 4843.
[2] G. Giannetto, A. Montes, N.S. Gnep, A. Florentino, P. Cartraud, M. Guisnet, J. Catal. 45 (1993) 86.
[3] P. Meriaudeau, G. Sapaly, C. Naccache, J. Mol. Catal. 81 (1993) 293.
[4] V.R. Choudhary, P. Devadas, A.K. Kinage, C. Sivadinarauana, M. Guisnet, J. Catal. 158 (1996) 537.
[5] K.J. Chao, S.P. Sheu, L.H. Lin, M.J. Genet, M.H. Feng, Zeolites. 18 (1997) 18.
[6] D.K. Simmons, R. Szostak, P.K. Agraval, T.L. Thomas, J. Catal. 106 (1987) 287.
[7] H. He, C.F. Cheng, S. Seed, T.L. Barr, J. Klinowski, J. Phys. Chem. 99 (1995) 3235.
[8] X.S. Liu, J. Lin, X.X. Liu, J.M. Thomas, Zeolites 12 (1992) 936.
[9] F.W. Lytle, R.B. Greegor, E.C. Marques, D.R. Sandstorm, G.H. Via, J.H. Sinfelt, J. Catal. 95 (1985) 546.
[10] E.A. Stern, M. Newville, Y. Yacoby, D. Haskel, Physica B. 208 (1995) 117.
[11] J.J. Rehr, J. Mustre de Leno, S.I. Zabinsky, R.C. Alberts, J. Am. Chem. Soc. 113 (1991) 5135.
[12] W. Kohn, L. Sham, J. Phys. Rev. A. 140 (1965) 1133.
[13] A.D. Becke, J. Chem. Phys. 98 (1993) 5648.
[14] C. Lee, W. Yang, R.G. Parr, Phys. Rev. B. 37 (1988) 785.
[15] M.J. Frisch, G.W. Trucks, H.B. Schlegel, G.E. Scuseria, M.A. Robb, J.R. Cheeseman, V.G. Zakrzewski, J.A. Montgomery Jr., R.E. Stratmann, J.C. Burant, S. Dapprich, J.M. Millam, A.D. Daniels, K.N. Kudin, M.C. Strain, O. Farkas, J. Tomasi, V. Barone, M. Cossi, R. Cammi, B. Mennucci, C. Pomelli, C. Adamo, S. Clifford, J. Ochterski, G.A. Petersson, P.Y. Ayala, Q. Cui, K. Morokuma, D.K. Malick, A.D. Rabuck, K. Raghavachari, J.B. Foresman, J. Cioslowski, J.V. Ortiz, A.G. Baboul, B.B. Stefanov, G. Liu, A. Liashenko, P. Piskorz, I. Komaromi, R. Gomperts, R.L. Martin, D.J. Fox, T. Keith, M.A. Al-Laham, C.Y. Peng, A. Nanayakkara, C. Gonzalez, M. Challacombe, P.M.W. Gill, B. Johnson, W. Chen, M.W. Wong, J.L. Andres, C. Gonzalez, M. Head-Gordon, E.S. Replogle, J.A. Pople, Gaussian98, Gaussian, Inc., Pittsburgh PA, 1998.
[16] J.B. Higgins, R.B. LaPierre, J.L. Schlenker, A.C. Rohrman, J.D. Wood, G.T. Kerr, W.J. Rohrbargh, Zeolites 8 (1988) 446.
[17] M.M.J. Treacy, J.M. Newsam, Nature 332 (1988) 249.
[18] W.M. Meier, D.H. Olson, Ch. Baerlocher, Atlas of Zeolite Structure Types, fourth ed., Elsevier, New York, p. 62.
[19] CERIUS^2, Molecular Modelling Software for Materials Research, Molecular Simulations, San Diego, CA.
[20] J.M. Newsam, M.M.J. Treacy, W.T. Koetsier, C.B. deGruyter, Proc. R. Soc. London A420 (1988) 375.
[21] K. Nishi, K.I. Shimizu, M. Tabamatzu, H. Yoshida, A. Satsuma, T. Ranaka, S. Yoslida, T. Hattori, J. Phys. Chem. B 102 (1998) 10190.
[22] G.L. Price, V.J. Kanazirev, Catal. 126 (1990) 267.
[23] K.J. Chao, A.C. Wei, H.C. Wu, J.F. Lee, Micropor. Mesopor. Mater. 35–36 (2000) 413.
[24] S.J. Geller, Chem. Phys. 33 (1960) 676.
[25] G.D. Meitzner, F. Iglesia, J.E. Baumgartner, E.S. Huang, J. Catal. 140 (1993) 209.
[26] K. Okabe, N. Matsuboayashi, Bull. Chem. Soc. Jpn. 64 (1991) 2602.